Vertical transmission of maternal DNA through extracellular vesicles associates with altered embryo bioenergetics during the periconception period

David Bolumar[1*], Javier Moncayo-Arlandi[2*], Javier Gonzalez-Fernandez[2], Ana Ochando[2], Inmaculada Moreno[2], Ana Monteagudo-Sanchez[2], Carlos Marin[1], Antonio Diez[1], Paula Fabra[3], Miguel Ángel Checa[3,4], Juan José Espinos[3,5], David K. Gardner [6,7], Carlos Simon[2,8,9±#], Felipe Vilella[2±#]

[1]Igenomix Foundation, INCLIVA Health Research Institute, Valencia, Spain

[2]Carlos Simon Foundation, INCLIVA Health Research Institute, Valencia, Spain

[3]Clinica Fertty, Barcelona, Spain

[4]Department of Medicine and Life Sciences, University Pompeu Fabra, Barcelona, Spain

[5]Department of Pediatrics, Obstetrics and Gynecology, School of Medicine, UAB, Bellaterra, Spain

[6]School of Biosciences, University of Melbourne, Australia

[7]Melbourne IVF, East Melbourne, Australia

[8]Department of Pediatrics, Obstetrics and Gynecology, School of Medicine, University of Valencia, Valencia, Spain

[9]Department of Obstetrics and Gynecology, BIDMC, Harvard University, Boston USA

* Contributed equally to this work.

[±] These authors are co-last authors

[#] Correspondence: csimon@fundacioncarlossimon.com, fvilella@fundacioncarlossimon.com

Word Count: 7346

Abbreviations: AB, apoptotic body; DLS, dynamic light scattering; EF, endometrial fluid; EVs, extracellular vesicle; EXO, exosome; mtDNA, mitochondrial DNA; MV, microvesicle; NTA, nanoparticle tracking analysis; OCR, oxygen consumption rate; TEM, transmission electron microscopy

Summary

The transmission of DNA through extracellular vesicles (EVs) represents a novel genetic material transfer mechanism that may impact genome evolution and tumorigenesis. We aimed to investigate the potential for vertical DNA transmission within maternal endometrial EVs to the pre-implantation embryo and describe any effect on embryo bioenergetics.

We discovered that the human endometrium secretes all three general subtypes of EV - apoptotic bodies (ABs), microvesicles (MVs), and exosomes (EXOs) - into the human endometrial fluid (EF) within the uterine cavity. EVs become uniformly secreted into the EF during the menstrual cycle, with the proportion of different EV populations remaining constant; however, MVs contain significantly higher levels of mitochondrial (mt)DNA than ABs or EXOs. During the window of implantation, MVs contain an eleven-fold higher level of mtDNA when compared to cells-of-origin within the receptive endometrium, which possesses a lower mtDNA content and displays the upregulated expression of mitophagy-related genes. Furthermore, we demonstrate the internalization of EV-derived nuclear-encoded (n)DNA/mtDNA by trophoblast cells of murine embryos, which associates with a reduction in mitochondrial respiration and ATP production.

These findings suggest that the maternal endometrium suffers a reduction in mtDNA content during the preconceptional period, that nDNA/mtDNA become packaged into secreted EVs that the embryo uptakes, and that the transfer of DNA to the embryo within EVs occurs alongside the modulation of bioenergetics during implantation.

Keywords: maternal-embryonic crosstalk, endometrium, exosomes, extracellular vesicles, metabolism, microvesicles, mitochondrial DNA,

Introduction

The release and uptake of membrane-enclosed compartments with specific cargos, commonly known as extracellular vesicles (EVs), represents a critical cell-to-cell communication mechanism (Niel et al., 2018). EVs support the transport of molecules and their protection from the extracellular environment (Niel et al., 2018) under both physiological and pathological conditions (Simón et al., 2018). EVs are generally classified into three populations based on their biogenic pathways, composition, and physical characteristics: apoptotic bodies (ABs), microvesicles (MVs), and exosomes (EXOs) (Andaloussi et al., 2013). All EV subtypes protect and transport nucleic acids, including all known types of RNA (Balkom et al., 2015; Huang et al., 2013; Valadi et al., 2007; Vojtech et al., 2014) and DNA (Lázaro-Ibáñez et al., 2014; Thakur et al., 2014a; Waldenström et al., 2012).

Endometrial EVs secreted into the endometrial fluid (EF) participate in embryo development (Burns et al., 2014, 2016; Ruiz-González et al., 2015), embryonic implantation (Greening et al., 2016; Ng et al., 2013; Vilella et al., 2015), trophoblast migration (Desrochers et al., 2016), and endometrial angiogenesis (Bidarimath et al., 2017; Salomon et al., 2014) during the periconceptional period. Micro(mi)RNAs represent the human endometrium's most widely studied EV cargo. The Salomonsen group first identified miRNAs as a cargo of endometrial epithelium-secreted EXOs, with the contained miRNAs found to target genes involved in embryonic implantation (Ng et al., 2013). Our studies revealed that the human endometrium secretes EXOs containing miRNAs with distinct menstrual cycle phase-related profiles into the EF (Vilella et al., 2015). We discovered that miR-30d uptake by the embryo promotes the expression of genes encoding factors involved in embryo adhesion. Additional studies suggest that both the embryo and the maternal endometrium release specific sets of miRNAs with transcriptional/epigenetic-modifying potential that participate in embryo viability, implantation, and uterus preparation during the preconception period (Ashary et al., 2018; Gross et al., 2017; Liang et al., 2017).

Evidence regarding DNA transmission through EVs also suggests that specific sorting of DNA molecules may occur depending on the cell type, EV subpopulation (Lázaro-Ibáñez et al., 2014), and ability of EVs to carry DNA to target cells (Waldenström et al., 2012). EVs contain single- and double-stranded DNA in varying relative abundances depending on the cell and vesicle type (Thakur et al., 2014b). The vertical transmission of EV-derived DNA has been proposed as a novel genetic material transfer mechanism that impacts genome

evolution (Kawamura et al., 2017). In support of this proposal, studies have indicated the involvement of the horizontal transfer of EV-derived DNA (especially involving retrotransposons) in tumorigenesis (Kawamura et al., 2017). Interestingly, EVs also transport mitochondrial (mt)DNA, constituting a mechanism to transmit normal or mutant mtDNA associated with specific pathologies from cell to cell (Guescini et al., 2010). For example, T-cell-derived EXOs secreted upon antigen-dependent contact with dendritic cells can transfer nuclear-encoded (n)DNA and mtDNA unidirectionally to dendritic cells, triggering resistance to subsequent viral infections (Torralba et al., 2018).

Here, we investigated the vertical transmission of DNA encapsulated within EVs secreted from cells of the endometrium to the embryo and explored the possible consequences of this process. Our data demonstrate that all EV subtypes encapsulate nDNA and mtDNA and that the endometrium releases MVs that specifically encapsulate an elevated amount of mtDNA during the receptive phase of the menstrual cycle. Embryos display evidence of EV-derived DNA uptake during the periconceptional period, which associates with an increased metabolic rate of the embryos and suggests a role in bioenergetic modulation.

Results

Morphological, molecular, and nanoparticle tracking-mediated identification of endometrial EV populations secreted into the endometrial fluid

We first isolated EV subpopulations from EF samples obtained at distinct time points during the female menstrual cycle to investigate those EVs secreted by the endometrium. We analyzed EVs using transmission electron microscopy (TEM), protein marker expression, dynamic light scattering (DLS), and nanoparticle tracking analysis (NTA).

During the receptive phase (phase IV of the natural menstrual cycle), we identified the existence of ABs from EF samples in sizes ranging from 1.5 µm to 8 µm (**Figure 1A** and **Supplementary Figures 1A** and **B**), which appeared as a multimodal population of two main sizes in DLS analysis (Note: NTA could not be used to measure AB concentration due to their large size). A main AB population displayed a mean size of 2,029 nm and accounted for 61.6% of total measured particles, while a second population displaying a mean size of 274.7 nm accounted for 38.4% of total particle content (**Figure 1B**). ABs expressed all AB/MB

molecular marker proteins evaluated (i.e., ARF6, VDAC1, Calreticulin, Calnexin, TSG101, CD63, and CD9) due to their heterogeneous origin (**Figure 1C**), while the detection of membranous-like structures within ABs (**Supplementary Figure 1B, Image 3**) suggested that this EV population also encapsulated different organelle structures. While these structures may represent mitochondria, we could not study their presence with organelle-specific markers.

MVs displayed sizes ranging from 200-700 nm and possessed a heterogeneous electron-dense content, as noted by TEM (**Figure 1D** and **Supplementary Figure 1C, Image 3**). MVs existed as a single population (98.7%) with a mean size of 290.8 nm by DLS (**Figure 1E**) and expressed specific molecular marker proteins (i.e., Calnexin, Calreticulin, ARF6, CD9, CD63, TSG101, and VDAC1) (**Figure 1F**). We observed an average MV concentration of $3.27 \cdot 10^9 \pm 6.22 \cdot 10^8$ part/mL, as analyzed by NTA (**Supplementary Figure 2A**).

TEM demonstrated the existence of homogeneously-structured EXOs in sizes ranging from 40–160 nm (**Figure 1G** and **Supplementary Figure 1D**). EXOs existed as a single-sized population (95.8%) (partially overlapping with MVs) with a mean size of 143.2 nm by DLS (**Figure 1H**) and expressed the EV-specific markers CD9, CD63, and TSG101 (**Figure 1I**). Finally, EXOs displayed a similar abundance as MVs ($3.18 \cdot 10^9 \pm 2.31 \cdot 10^8$ part/mL), as analyzed by NTA (**Supplementary Figure 2B**).

We also measured the relative abundances of secreted MVs and EXOs across the menstrual cycle (**Figure 1J** and **K**) (as mentioned before, ABs cannot be measured using NTA). MV concentrations remained similar throughout the menstrual cycle (**Figure 1J**), ranging from minimal levels in the post-receptive phase (phase V) ($5.26 \cdot 10^7 \pm 1.65 \cdot 10^7$ part/mL) to maximal in the proliferative phase (phase I) ($3.48 \cdot 10^8 \pm 2.03 \cdot 10^8$ part/mL) (**Supplementary Figure 3A**). EXO concentrations displayed greater variability throughout the menstrual cycle, although these changes remained non-significant (**Figure 1K**); overall, the number of particles secreted per ml did not significantly change (**Supplementary Figure 3B**).

In summary, we discovered that the human endometrium secretes the three major EV subtypes and that the concentration of MVs and EXOs secreted into the EF does not significantly change during the different phases of the menstrual cycle.

Sequencing of endometrial EV-derived DNA isolated during the periconception period

Next, we sequenced the DNA content of EF-derived EV populations (n=10) isolated during the periconceptional period (receptive endometrium, phase IV). We first used DNase pre-treatment of EVs to ensure bona fide DNA content for sequencing (**Supplementary Figures 4A and 4B** and **Materials and Methods**). We compared the coding sequences obtained from isolated EVs with the ENSEMBL database, revealing the homogenous and more differentiated nature of ABs compared to MVs and EXOs, which possessed a more dispersed overlapping distribution. The grouping together of AB samples indicates a similar content, which differs from other EV subtypes. ABs, mainly generated by apoptotic cells, typically display greater homogeneity than MVs or EXOs, given their large size and the encapsulation of a greater amount of intracellular material, making their contents less specific (**Supplementary Figure 4C**).

All EV subtypes can encapsulate DNA, and we analyzed if any differences existed regarding DNA content using paired comparisons, with results displayed as volcano plots. MVs displayed significant differences regarding DNA content compared to ABs (**Figure 2A**) and EXOs (**Figure 2B**), while ABs and EXOs displayed no significant differences (data not shown). This suggests that MVs contain more specific DNA sequences than other EVs, as shown in volcano plots regarding FWER ($\alpha < 0.05$) and >2 fold-change.

While elucidating the specific sequences of DNA encapsulated within EVs, we observed an average 11.12±0.53-fold change enrichment in thirteen specific known mitochondrial genes in MVs compared with EXOs (**Figure 2C**). MVs also displayed enrichment for two mitochondrial pseudogenes and a long intergenic non-coding RNA from the Chr1:536816-659930 genomic region compared to EXOs, and a mitochondrial pseudogene and three protein-coding genes from different genomic loci compared to ABs (**Figure 2C**).

These results demonstrate that all EVs generally encapsulate DNA (nDNA and mtDNA), although MVs contain higher levels of mtDNA than ABs and EXOs.

Endometrial EVs encapsulate mtDNA while mtDNA levels become reduced in the receptive endometrium

To understand the encapsulation of mtDNA in EVs and their secretion by endometrial cells, we analyzed the relative mtDNA content compared to the nDNA content of endometrial tissue biopsies from women undergoing hormone replacement therapy (HRT) during the receptive or periconceptional period (P+5). We analyzed receptivity status using the

179 endometrial receptivity analysis (ERA) test (n=70), which demonstrated the number of
180 women in pre-receptive, receptive or periconceptional, and post-receptive periods. We
181 quantified the ratio between mtDNA/nDNA content using qRT-PCR, as previously described
182 (Diez-Juan et al., 2015). We observed a significant reduction (both $p<0.001$) of mtDNA in
183 receptive (n=25) and post-receptive endometria (n=23) compared to the pre-receptive (n=22)
184 phase (**Figure 3A**); furthermore, the post-receptive endometrium displays a significantly
185 lower content of mtDNA compared to the receptive endometrium ($p<0.001$).

186 We then sought to understand the mechanisms underlying the reduction of mtDNA levels in
187 the periconceptional/receptive endometrium using the same HRT patient samples. Previous
188 research has linked the activation of the cellular mitochondrial degradation and recycling
189 system (autophagy) to the encapsulation of mtDNA into EVs and their subsequent release
190 into the extracellular space (Kumar et al., 2014). Therefore, we investigated the expression of
191 genes that regulate specific pathways involved in mitochondrial autophagy (mitophagy) and
192 engulfment into autophagosome for degradation in the pre-receptive, receptive, and post-
193 receptive endometrium (Youle and Narendra, 2011). We found that vesicular targeting
194 receptors Sequestosome-1 (SQSTM1) and Microtubule-associated proteins 1A/1B light chain
195 3A (MAP1LC3A) and the mitophagy inductor PTEN-induced kinase 1 (PINK1) became
196 significantly upregulated in the receptive and post-receptive stages when compared to the
197 pre-receptive stage ($p<0.001$) (**Figure 3B**). We also observed the significantly downregulated
198 expression of constitutive components of the mitochondria, such as the ribosomal protein S16
199 (MRPS16), mitochondrial ribosomal protein S9 (MRPS9), and mitochondrial import receptor
200 subunit 22 (TOMM22), when comparing the pre-receptive stage to the receptive and post-
201 receptive stage ($p<0.001$) (**Figure 3B**); these data may indicate a decrease in mitochondrial
202 mass, which again coincides with a higher mtDNA content in secreted MVs.

203 As MVs possess a considerable content of mtDNA during the receptive phase, we measured
204 the mtDNA copy number content in EF-derived MVs from patients undergoing HRT in the
205 pre-receptive, receptive or periconceptional period, and post-receptive periods to compare
206 against the findings from endometrial samples. Quantifying mtDNA copy number in MVs
207 demonstrated the accumulation of mtDNA during the receptive compared to the pre-receptive
208 period. Specifically, we found a 3.2-fold enrichment in mtDNA copy number in MVs in the
209 receptive compared to the pre-receptive period and a 2.6-fold enrichment in the post-

receptive compared to the pre-receptive period (**Figure 3C**); however, these changes failed to reach significance.

Altogether, these data indicate a reduction in mtDNA content and the activation of mitochondrial clearance mechanisms in the human endometrium at times associated with embryo implantation alongside the secretion of mtDNA in endometrial MVs.

Vertical transmission of EV-derived DNA from the maternal endometrium to the embryo

To provide evidence for the internalization of EVs (and associated DNA) by murine embryos, we used the endometrial Ishikawa cell line to produce EVs containing DNA tagged with a synthetic molecule (**Materials and Methods**) to support the tracking of EV-derived DNA uptake. Before confocal experiments, we first confirmed the ability of DNA to become internalized by EVs/packaged into EVs by flow cytometry (**Supplementary Figure 5**). Confocal imaging demonstrated that ABs released from Ishikawa cells effectively transported DNA into the cells of the embryo, reaching the cytoplasm (**Figure 4**) and colocalizing with nuclei (Arrows in **Supplementary Figure 6**). A considerable amount of AB-delivered DNA accumulated in large deposits in discrete zones of the embryo, but mainly in the cytoplasm (**Figure 4**). MVs delivered DNA into the trophectoderm of the embryo (**Figure 4** and **Supplementary Figure 6**), with DNA transmission occurring in a widespread spotted pattern at the perinuclear level. We also observed evidence for the delivery of DNA into the embryo cell cytoplasm and nuclei by EXOs; of note, the small size of EVs makes their robust imaging more challenging than for ABs and MVs (**Figure 4** and **Supplementary Figure 6**). Regardless of the subtype, EV-derived DNA internalized into hatched trophectoderm (sites where direct contact is possible) (**Figure 4**). The control conditions (**Figure 4 -** Neg), which contained cell-free DNA and residual small-sized EVs, failed to demonstrate any detectable signal indicating the transfer of DNA into the cells of the embryo, suggesting that DNA transport from the mother to the embryo at the endometrial level requires EVs (**Figure 4**). As final proof of the internalization of EV-derived DNA into the cytoplasm/nuclei of embryo cells, we constructed Z-stack/orthogonal projection images (**Supplementary Figure 6**). To prove the internalization of mtDNA, we analyzed the incorporation of free (not encapsulated within EVs or other artificial vesicles) synthetic molecules of labeled mtDNA within embryos using confocal microscopy; overall, we also observed robust mtDNA internalization by trophectodermal cells of hatched embryos (**Supplementary Figure 7**).

Overall, we demonstrate that DNA-containing EVs generated by human endometrial cells become internalized by the trophectoderm of murine embryos in vitro.

Bioenergetic impact of endometrial EV-derived DNA uptake by the embryo

To assess the functional relevance of vertical endometrial EV-derived DNA transmission and the impact on embryo bioenergetics, we analyzed ATP concentrations in cells of the embryo. We co-cultured overnight hatched murine blastocysts with different human EF-derived EV populations (either separately or combined) derived from five donors during the receptive phase of the menstrual cycle and compared results with those from embryos cultured in the absence of endometrial EVs (Control, Cnt). We found a significant reduction in ATP levels following embryo co-culture with "All EVs" or EXOs compared to control embryos (both $p<0.001$) (**Figure 5A**); however, murine embryos incubated with only ABs or MVs from human EF maintained ATP levels similar to control ($p>0.05$). These results suggest that EVs (EXOs in particular) significantly impact ATP consumption/production in the embryo. The observed reduction in ATP concentration after exposure to "All EVs" and EXOs indicates an increase in cellular metabolic rate; therefore, embryos display ATP turnover after internalizing endometrial EVs, a situation that imitates the physiological state at periconception when the embryo comes into contact with the EF and EVs secreted by the endometrium.

To further understand the metabolic changes produced by EVs on the embryo, we studied the oxygen consumption rate (OCR) of embryos, as the manipulation of microenvironmental parameters to help uterine implantation represents a well-understood first signal from the blastocyst to the endometrium (Gardner, 2015; Gardner and Harvey, 2015; Gurner et al., 2022). We studied the effect of endometrial EVs by analyzing the OCR of embryos incubated with EF-derived MVs and EXOs (**Figure 5B**). We observed a reduction in the OCR of embryos treated with EXOs obtained from donors in the receptive phase (P+5) compared with the pre-receptive phase (P+2) (basal respiration and maximal respiration) (**Figure 5B-D**); while this reduction did not reach significance (perhaps due to the small sample size), the result paralleled the results observed for ATP consumption, potentially reflecting an increase in glycolytic flux. Of note, MVs appeared not to alter OCR (basal respiration and maximal respiration) in embryos (**Figure 5B-D**). Arrested embryos used as negative control (neg Cnt) did not respond to drug stimulation, indicating the viability of the embryos evaluated in this experiment.

These results suggest that EVs play a role in altering the bioenergetics of the embryo by altering the metabolic rate and oxygen consumption during periconception when a move towards increased glycolytic flux to support implantation is required. These results suggest that the endometrium may exchange signals with the embryo to aid the creation of conditions conducive to implantation.

Discussion

We demonstrate the existence of endometrial EVs as potential vectors for the transport of DNA from the endometrium into the pre-implantation embryo; furthermore, our results suggest the vertical transmission of maternal DNA to the embryo as a mechanism to modulate embryo bioenergetics during the preconception period. These findings pave the way for more extensive, more detailed studies that aim to decipher the exact role of EV contents on embryo energetics, discover the relevance of packaged endometrial cell-derived DNA to this mechanism, and further expand our knowledge regarding materno-fetal communication.

We discovered that human endometrial cells secreted the three major EV subtypes into the EF during the receptive phase (phase VI) and characterized ABs, MVs, and EXOs morphologically using electron microscopy, molecularly using Western blotting, and by concentration and size distribution. In the case of MVs and EXOs, we identified similar concentrations in the EF throughout the menstrual cycle.

While other studies focused on the miRNA and protein content of EVs, we focused on the DNA cargo. We sequenced the DNA content of ABs, MVs, and EXOs isolated from the EF and found that all vesicles contained nDNA and mtDNA; however, MVs contained an ~11-fold enrichment in thirteen known mitochondrial genes (all coding for protein subunits that constitute the different complexes of the electron transport chain (Chinnery and Hudson, 2013; Taanman, 1999)). To understand the increased encapsulation of mtDNA within EVs, we quantified the mtDNA content of cells from endometrial biopsies, focusing on the possible differences between the pre-receptive, receptive, and post-receptive phases of the menstrual cycle. We observed a decrease in mtDNA content in endometrial cells during the receptive and post-receptive phases, which occurred at the same time as the upregulation of specific genes related to mitochondrial autophagy (SQSTM1, MAPILC3A, and PINK1), suggesting the existence of mitochondrial degradation in the endometrial tissue, coincident with the maximum encapsulation of mtDNA by MVs. Holmgren et al. described a role for

ABs in the horizontal transfer of DNA by phagocytosis, which the authors found to integrate into receiving cells and remain functional, as they can be rescued from the ABs and used by somatic cells (Holmgren et al., 1999). ABs support the formation of DNA molecular hybrids or hybrid chromosomes (Bergsmedh et al., 2001; Waterhouse et al., 2011) and transfer oncogenes that become internalized to increase target cell tumorigenic potential in vivo (Bergsmedh et al., 2001; Ehnfors et al., 2009). MVs also represent critical regulators of cancer pathogenesis (Antonyak et al., 2011; Clancy et al., 2015) in addition to their involvement in materno-fetal crosstalk (Tong and Chamley, 2015) and embryo self-regulation (Desrochers et al., 2016). Finally, EXOs play multiple roles in many biological processes; however, small RNA delivery (mainly miRNA) represents their primary function (Valadi et al., 2007; Villarroya-Beltri et al., 2013). The role of EVs in materno-fetal crosstalk and reproductive biology has been extensively analyzed (Greening et al., 2016; Lee et al., 2015; Vilella et al., 2015). Interestingly, EXOs also play a role in packaging and transferring mtDNA from patients with hormonal therapy-resistant metastatic breast cancer, which participates in the oncogenic signaling that induces cancer cells to exit dormancy (Sansone et al., 2017).

EVs containing DNA must first become internalized by trophectodermal cells to influence the embryo in any way. We demonstrated the internalization of ABs, MVs, and EXOs by murine embryos using labeled DNA tracked by confocal microscopy. In all experiments, we observed the internalization of EVs by the trophectodermal cells of murine embryos. ABs delivered substantial amounts of genetic material that occupied large but discrete regions of the embryo. In contrast, the MV-mediated DNA transmission pattern appeared widespread throughout the embryo as small perinuclear spots; meanwhile, EXOs also demonstrated potential for vertical DNA transfer.

Considering the DNA content of EVs and their uptake by the embryo, we evaluated a potential effect on embryo energetics. We hypothesized that maternal signals might regulate embryo bioenergetics to aid implantation (Gardner, 2015; Gardner and Harvey, 2015). Embryo co-culture with "All EVs" (ABs, MVs, and EXOs) induced a lower ATP content than unstimulated controls, suggesting that the internalization of DNA (which includes the prevalent mtDNA content) may impact ATP consumption, which directly associates with the metabolic programming of embryos (Gardner and Harvey, 2015). We primarily observed the substantial reduction of ATP content when co-culturing murine embryos with isolated EXOs,

suggesting that a combination of contents (e.g., DNA, RNA, proteins, and lipids) controls the metabolic state of embryos. Additional studies will aim to fully explore each EV cargo's potential contribution. We next studied the OCR of the embryos treated with EXOs and MVs from the pre-receptive and receptive phases (we removed ABs from this analysis due to their heterogeneity and methodological difficulties). We observed that EXOs obtained from receptive but not pre-receptive endometria appeared to reduce basal respiration (while not reaching significance), similar to the changes to ATP levels when treating embryos with "All EVs" or EXOs. Again, future studies with more samples may reveal the real significance of these effects and decipher the exact role of each EV subtype and their cargos.

We suggest EVs as vectors for transporting nDNA and mtDNA into the pre-implantation embryo; this maternal DNA vertical transfer mechanism could influence embryo metabolism during the periconceptional period, suggesting that the mother sends signals to the embryo to aid the implantation process.

Methods

Experimental design

EF samples were collected from women undergoing natural (healthy volunteers aged 18–35) cycles and women undergoing hormonal replacement therapy. EF samples for the natural menstrual cycle were collected from each donor (one from each) and classified according to the menstrual cycle as phase I (early proliferative, days 0–8 (n =6)), phase II (late proliferative, days 9–14 (n = 7)), phase III (early secretory, days 15–18; (n = 7)), phase IV (mid-secretory or preconception period, days 19–24; n = 36), and phase V (late secretory phase, days 25–30; (n = 6). Additional sets of EF samples were collected from women undergoing hormonal replacement therapy in pre-receptive (P+2), receptive (P+5), or post-receptive (P+8) stages (n=12 donors; three collections/donor) for a total of n=30 EF. The total number of EF samples collected for this study was n=62. Endometrial biopsies were collected from women undergoing hormonal replacement therapy in receptive (P+5) stages (n=70). The number of samples used in every experiment is specified throughout the methods section.

Inclusion criteria were patients with regular menstrual cycles, body mass index (BMI) of 18–30 kg/m^2, no contraceptive devices or hormonal treatment in the past three months, negative

for bacterial/viral infectious diseases, and without obvious uterine or adnexal pathologies. The IRB committee approved this study at IVI Valencia, Spain (1603-IGX-017-FV and IGX1-VES-FV-21-04), and all subjects provided signed informed consent.

Endometrial fluid sampling

After cleansing the vaginal channel, EF samples were obtained from the uterine fundus using a double lumen embryo transfer catheter (Wallace, Smiths Medical International, Minneapolis, MN, USA) introduced into the uterine cavity and applying gradual suction using a 10 mL syringe. The vacuum was stopped to prevent contamination with cervical mucus, the catheter was gently removed, and EF was introduced in an Eppendorf tube for storage at -80ºC until processing.

EV isolation from endometrial fluid

Each EF sample was resuspended in 1 mL of cold (4ºC) Dulbecco's PBS without Ca^{2+}/Mg^{2+} (L0615-500; Biowest, Barcelona, Spain) to prevent salt precipitation. Resuspensions were homogenized by extensive pipetting and vortex, and samples were treated with 50 U/mL DNase type I (D4513; Sigma-Aldrich, Madrid, Spain) to disaggregate mucus and eliminate extravesical DNA. For EV isolation, each resuspended EF sample volume was increased to 4 mL with PBS, and samples underwent a series of differential centrifugations and filtration; centrifuged twice at 300 x *g* for 10 min to pellet residual cells and debris, with the resulting supernatants centrifuged at 2,000 x *g* for 10 min, passed through 0.8 µm-diameter filters (GE Healthcare, Life Sciences, Whatman, UK), centrifuged at 10,000 x *g* for 30 min, passed through 0.22 µm-diameter filters (Acrodisc syringe filters, Pall Corp., Newquay, Cornwall, UK), and ultracentrifuged at 120,000 x *g* for 70 min using a P50AT4 rotor (Hitachi Koki Co. Ltd., Tokyo, Japan). Pellets were washed in 1 mL PBS and centrifuged again under the same conditions to obtain fractions subsequently enriched in ABs (2,000 x *g* for 15 min), MVs (10,000 x *g* for 40 min), and EXOs (120,000 x *g* for 70 min, using a Hitachi P50A3 rotor). The resulting supernatants were kept as negative controls. All centrifugations were carried out at 4ºC.

Transmission electron microscopy

Pellets from serial differential centrifugations of single EF samples (n = 4, 2 per each technique) obtained in phase IV of the natural cycle were analyzed by two TEM techniques.

Deposition and positive staining (to evaluate external aspects and preliminary size): Pellets were resuspended in 50 µL of Karnovsky's fixative solution (2.5% glutaraldehyde/2% formaldehyde in 0.1 M phosphate buffer, pH = 7.4), and a drop of the resulting mix was laid onto a 300-mesh grid. Samples were then incubated with 2% uranyl acetate in Reynold's lead citrate solution (80 mM lead nitrate, 120 mM sodium citrate dihydrate, and 100 mM NaOH in distilled water).

Inclusion in LR-white resin and ultrathin cuts (to evaluate EV internal structures and general contents): Isolated pellets were carefully fixed in 50 L of Karnovsky's solution without disturbing the pellet. Fixed pellets were washed five times in PBS for 5 min each and stained in a 2% osmium tetroxide/0.2 M PBS solution for 2 h. Samples were dehydrated, embedded in resin (Epoxy), and ultra-sectioned in 60-nm slices. Samples were observed using a JEM-1010 TEM (Jeol Korea Ltd., Seoul, South Korea) at 80 kV coupled to a digital camera MegaView III.

Western blotting

EV populations isolated from phase IV of natural cycle human EF (n = 3) were lysed in 50 L of RIPA buffer (150 mM NaCl, 1% IGEPAL CA 630, 0.5% Na-DOC, 0.1% SDS, 0.5 M EDTA, 50 mM Tris-HCl, pH 8) prepared with protease inhibitors [89% RIPA, 1% 0.1 M PMSF (Sigma-Aldrich, Madrid, Spain), 10% Roche Mini Complete (Roche, Madrid, Spain)]. The protein content of EV samples, supernatants obtained during EV isolation, and tissue cell lysates were quantified by Bio-Rad Protein Assay (Bio-Rad Laboratories, Hercules, CA, USA). The cell lysate was generated as a Western blot positive control from the human endometrial epithelium Ishikawa cell line (Sigma-Aldrich, Madrid, Spain), as in a previous study (Vilella et al., 2015). Equal protein amounts were denatured at 95ºC, electrophoresed by SDS-PAGE, and transferred to PVDF membranes (Bio-Rad Laboratories).

Membranes were blocked in 5% skim milk in 1% Tween-20 in PBS (PBS-T) and incubated overnight at 4ºC with the following primary antibodies: rabbit anti-calnexin (1:1,000; ADI-SPA-865; Enzo Life Sciences, Farmingdale, NY, USA), mouse anti-calreticulin (1:1,000; ab22683; Abcam, Cambridge, UK), rabbit anti-VDAC1 (1:1,000; ab154856; Abcam), rabbit anti-ARF6 (1:1,000; ab77581; Abcam), mouse anti-CD63 (1:1,000; ab59479; Abcam), rabbit anti-CD9 (1:1,000; ab92726; Abcam), and rabbit anti-TSG101 (1:1,000; 125011; Abcam). The following day, membranes were washed and incubated with secondary antibodies: goat

anti-mouse (1:10,000; sc-2005; Santa Cruz Biotechnology, Dallas, TX, USA) or goat anti-rabbit (1:20,000; EXOAB-KIT-1; System Biosciences, Palo Alto, CA, USA). Protein signals were detected using the SuperSignal West Femto Chemiluminescent kit (Thermo Fisher Scientific, Waltham, MA, USA) and a LAS-3000 imaging system (Fujifilm, Japan).

Dynamic light scattering

Two EF samples were used for the ZetaSizer Nano (Malvern Instruments Corp., Malvern, UK), a device based on dynamic light scattering (DLS) technology, which was used to generate general size distribution patterns of the different EV fractions in a wide size range (1–6,000 nm). For analysis, pellets from serial differential centrifugation steps were resuspended in 1 mL of PBS without Ca^{2+}/Mg^{2+}, transferred to 4 mL polystyrene cuvettes, and analyzed on a Malvern ZetaSizer Nano□ZS 90.

Nanoparticle tracking analysis

EF samples for the natural menstrual cycle, phase I (early proliferative, days 0–8 (n =6)), phase II (late proliferative, days 9–14 (n = 7)), phase III (early secretory, days 15–18; (n = 7)), phase IV (mid-secretory or preconception period, days 19–24; n = 6), and phase V (late secretory phase, days 25–30; (n = 6). NanoSight 300 (Malvern Instruments Corp.), a technology based on nanoparticle tracking analysis (NTA) principles, was used to finely analyze EV size distribution and concentrations from EF samples throughout the menstrual cycle using light scattering properties. Due to its more limited size working range (up to 1,000 nm), ABs could not be analyzed. To normalize concentration measurements, EF volumes were measured prior to EV isolation so that we could refer to EV concentration per mL. Pellets containing isolated vesicles were resuspended in 1 mL PBS without Ca^{2+}/Mg^{2+} and introduced into the NanoSight 300.

High throughput sequencing of the DNA cargo from human endometrial EVs

To analyze the DNA cargo of the different EV populations within the human EF, EVs were isolated from single EF samples in phase IV (n=10) of the menstrual cycle as described above. To eliminate DNA stuck externally to the vesicles, isolated EVs were treated with 50 U/mL DNaseI (Sigma-Aldrich, ref. D4513) in a solution containing 20 mM Tris-HCl, 10 mM $MgCl_2$ and 1 mM $CaCl_2$ and incubated at 37ºC for 30 min while gently shaking. DNase type I pre-treatment was performed to ensure that bona fide DNA cargo was sequenced. To prove

the use of DNase, a total of six EF phase IV samples were pooled and separated in fractions and divided into three different groups: control group (no DNase), treated with DNaseI, and treated with DNaseI + exonuclease T5; the PCA for coding gene sequences demonstrated that DNase treatment accounted for 56% and 57% of the total variability for ABs and EXOs, respectively, in PC1 (**Supplementary Figures 4A and 4B**). Associated volcano plots revealed abundant enrichment in coding sequences over whole genomic DNA after DNase treatment (Yellow dots). These results indicated that external DNA contamination masks EVs DNA cargo, which should be prevented by DNase treatment to investigate specific EVs DNA inner cargo.

After digestion, DNaseI was heat-inactivated by incubating at 75ºC for 10 min at 2:30 v:v of 0.5M EDTA (Thermo Fisher Scientific, ref. 15575020). Next, DNA contained in EVs was extracted using the QIAamp DNA Mini Kit protocol for cultured cells (Qiagen, ref. 51306). Only samples that accomplished a minimum of 0.03 ng/µL of DNA in all the vesicle populations from the same EF were chosen for library construction. A lower threshold was chosen based on our previous experience. Samples over 0.2 ng/µL were adjusted to this concentration with nuclease-free water. To analyze the effect of lowering the DNA input amount for libraries construction (samples with initial limiting input DNA), those samples with DNA excess from the DNase evaluation assay (i.e., DNase untreated EXOs and ABs) were used to create serial dilutions for library construction. The resulting libraries containing an initial 0.05 ng/µL DNA and those in the ideal concentration range (0.2 ng/µL and 0.15 ng/µL for ABs and EXOs, respectively) were chosen to evaluate the effect of reducing DNA input for sequencing. The selection was based on the similarity of DNA concentrations and library profiles, measured by Bioanalyzer 2100 HS DNA assay (Affymetrix), between 0.05 ng/µL DNA dilutions and initial limiting DNA samples.

In all cases, libraries were constructed using the Nextera XT DNA Library Prep Kit (Illumina, ref. FC-131-1024) following the manufacturer's instructions. As variable parameters, libraries AMPure XP (Beckman Coulter, ref. 082A63881) purification was carried out at 1X, bead-based normalization was chosen, and, following Illumina's instructions, a 4 µL volume was chosen for serial dilution in 996 µL and 750 µL/750 µL in HT1. Finally, libraries were sequenced by an Illumina NextSeq 500 (Illumina) using a 300-cycle NextSeq 500 High Output v2 Kit cartridge (Illumina, ref. FC-404-2004).

DNA sequencing analysis

Raw data from pair-ended Illumina sequencing was converted into FASTQ files using bcl2fastq (version 2.16.0.10). Raw counts were normalized using the TMM method from the edgeR R package, and each sample was aligned to the reference genome (GRCh37) using BWA (version 0.7.10). Reads with mapping quality >90% were filtered using Samtools (version 1.1), and duplicates were removed with PICARD software. Insert size was retrieved from filtered reads using PICARD software, and feature coverage was obtained with Bedtools (version 2.17.0) using Ensembl Biomart hg19 annotations. For the following bioinformatics analysis, reads mapping to chromosome Y and noisy samples were filtered out. The approach used for differential DNA enrichment analysis was based on the edgeR methodology. PCA graphs were obtained from log2 normalized CPM using the prcomp R function for all samples and comparisons. Descriptive and Pearson's correlation analyses were carried out to analyze the effect of reducing initial DNA concentration.

Endometrial biopsies

All patients underwent an HRT cycle for endometrial preparation (n=70). Endometrial biopsies were collected from the uterine fundus using a pipette under sterile conditions. The day of the endometrial biopsy is calculated after estrogen priming, leading to a trilaminar endometrium measuring ≥6.5 mm after five full days of progesterone impregnation (~120 h). After the biopsy, the endometrial tissue was transferred to a cryotube containing 1.5 mL RNAlater (Qiagen), vigorously shaken for a few seconds, and kept at 4°C or on ice for ≥4 h. Determining the receptivity window used the ERA test, as previously described (Díaz-Gimeno et al., 2011). Biopsies were classified as receptive (n=25), pre-receptive (n=22), and post-receptive (n=23).

Determination of mitochondrial DNA copy number in biopsies

Relative amounts of nDNA and mtDNA were determined by quantitative RT-PCR as previously described (Diez-Juan et al., 2015). The nuclear gene β-actin was selected as a housekeeping gene for normalization. mtDNA was quantified using an mtDNA fragment within the ATP8 gene. The ratio of mtDNA/nDNA was used to indicate the mitochondrial copy number per cell.

Quantitative RNA sequencing in Biopsies

100 ng total RNA was reverse transcribed using the Ion AmpliSeq Transcriptome Human Gene Expression Kit following the manufacturer's protocol (Thermo Fisher Scientific). Target genes (SQSTM1, MAP1LC3A, PINK1, MRPS16, MRPS9, and TOMM22) were amplified using an Ion AmpliSeq Transcriptome Human Gene Expression Core Panel (Thermo Fisher Scientific). Amplicons were ligated to barcode adapters and purified using Agencourt AMPure XP reagent (Beckman Coulter Inc.). After purification, amplicons were eluted and normalized before emulsion PCR and chip loading on the Ion Chef system, obtaining reads with an average length of 200 bp. The sequencing data were aligned using the ampliSeqRNA plugin for Ion Torrent sequencing platforms (Thermo Fisher Scientific).

mtDNA copy number quantification in MVs

As detailed above, EVs isolated from EF (n=21) in different menstrual cycle stages (P+2 n=7, P+5 n=7, P+8 n=7) were DNase treated to eliminate extravesical DNA contamination. MVs-derived DNA was amplified using the Sureplex DNA amplification system (Illumina) according to the manufacturer's instructions. This amplification step increases the DNA yield obtained per sample to ensure a sufficient amount for qPCR analysis without altering the proportion of the different sequences. Samples were purified using AMPure XP beads (Beckman Coulter), and the DNA was quantified using D1000 ScreenTape in a TapeStation 4200 instrument (Agilent). Only DNA samples containing >0.1ng/µL were used for the qPCR analysis. The mitochondrial ATP8 gene was amplified in a qPCR machine using the following primers: Forward 5'-CTAAAAATATTAAACACAAACTACCACCTACCTC-3' and Reverse 5'-GTTCATTTTGGTTCTCAGGGTTTGTTATAA-3'. Standard curves were created by qPCR amplifying serial dilutions of the ATP8 amplicon and used to calculate the copy number of mtDNA in 250 pg of DNA per reaction. Half of the MVs samples were used to calculate the concentration of MVs by NTA analysis, and the mtDNA copy number was normalized with the number of MVs (mtDNA copy number/MV).

Murine embryo isolation and culture

Murine embryos were obtained from B6C3F1/Crl mice (Charles River Laboratories, Saint-Germain-Nuelles, France). The Animal Care and Use Committee of Valencia University (CEBA) authorized the project under the identifier: 2015/VSC/PEA/00048. The embryo recovery and culture processes were adapted from our previous work (Vilella et al., 2015). Briefly, female mice aged 6-8 weeks were stimulated to ovulate by 10 IU intraperitoneal

injection of Foligon/PMSG (MSD Animal Health, Spain) followed by intraperitoneal administration of 10 IU of Ovitrelle 250 µg/0.5 mL (Merck Serono, Germany) 48 h later. At that point, females were mated with males of the same strain for 48 h, checking for the presence of a vaginal plug. Plug-positive females were sacrificed by cervical dislocation, and embryos were collected from the oviduct by flushing with PBS using a 30-gauge blunt needle. Embryos were then washed four times in overnight oxygenated G-2 plus medium (G-2 PLUS, Vitrolife, Barcelona, Spain) and cultured until hatching for 48 h in the same medium (day E3.5 of embryo development). An average of 30-40 embryos per female were obtained, with 60% reaching the hatching state with excellent quality at E3.5.

Tagged-DNA production and EV internalization by murine embryos

The human Ishikawa were grown in flasks in Modified Eagle's Medium (MEM, Gibco, Thermo Fisher Scientific, ref. 10370021), supplemented with 5% fetal bovine serum (Biowest, Barcelona, Spain, ref. S181B-500), 1% non-essential amino acids (Gibco, Thermo Fisher Scientific, ref. 11140035), 1% Glutamax (Gibco, Thermo Fisher Scientific, ref. 35050-038), 0.2% 50 mg/mL gentamicin (Gibco, Thermo Fisher Scientific, ref. 15750-037) and 0.2% 250 µg/mL amphotericin B (Gibco, Thermo Fisher Scientific, ref. 15290026), until 60-70% confluence.

For the generation of EdU DNA-tagged EVs, three T175 flasks of Ishikawa cells at 60-70% confluence were supplemented with 1 µM 5-ethynyl-2'-deoxyuridine (EdU, Thermo Fisher Scientific) and incubated overnight to allow EdU incorporation into the DNA. The next day, cells were washed twice in PBS and added to the Ishikawa medium containing EV-depleted fetal bovine serum. Finally, conditioned media containing EVs was collected after 24 h, and the different EVs populations were isolated as described above.

Pellets containing Ishikawa EdU DNA-tagged EVs were added to good-quality E3.5 hatching embryos and co-incubated overnight. Twenty embryos were used for each condition (ABs, MVs, EXOs, and Neg), for a total of eighty embryos. The supernatant of the isolation process and a mixture of EVs populations generated by Ishikawa cells cultured in the absence of EdU were used as negative controls. After embryo co-culture with EVs, transferred EV-DNA was stained by click-it chemistry reaction using Click-iT™ EdU Alexa Fluor™ 488 Imaging Kit (Thermo Fisher Scientific, ref: C10337). The protocol was carried out as recommended by the manufacturers with some modifications. Embryos were fixed with 3.7% formaldehyde in

PBS solution and stained with Wheat Germ Agglutinin, Texas Red™-X Conjugate (Thermo Fisher Scientific, ref: W21405) for 20 min at 37ºC. After permeabilization in 0.5% Triton X-100 in PBS, embryos were labeled with EdU, rinsed in PBS, and stained with DAPI solution (Thermo Fisher Scientific, ref: 62248). Stained embryos were imaged with an FV1000 Olympus confocal microscope using a 60X oil-immersion lens.

The Click-iT™ EdU Alexa Fluor™ 488 flow cytometry assay Kit (Thermo Fisher Scientific, ref: C10420) was used to analyze EdU incorporation within the different EV subpopulations obtained from Ishikawa cells. A fraction of the isolated EVs from EdU-labelled and non-labeled Ishikawa cells were pelleted and resuspended with the Click-it Plus reaction cocktail following the manufacturer's instructions. After a washing step, EVs were analyzed in a cytoFLEX flow cytometer (Beckman Coulter), and the data were analyzed with FlowJo software.

mtDNA internalization by mouse embryos

Hatched mouse embryos (3.5 days) were co-culture with an ATP8 sequence (Forward: /5Biosg/ctaaaaatattaaacacaaactaccacctacctccctcaccaaagcccataaaaataaaaaattataacaaaccctgagaaccaaaatgaac; Reverse: /5Biosg/gttcattttggttctcagggtttgttataatttttattttatgggctttggtgagggaggtaggtggtagtttgtgtttaatattttta g) conjugated with Biotin (manufactured by IDT) overnight at 37ºC and 5% CO_2. Embryos were permeabilized with 0.1% Triton-X-100 in PBS for 20 min, blocked with 3% bovine serum albumin in PBS for 30 min shaking, incubated with Streptavidine-Cy3 (S6402, Merck; dilution 1:100) for 45 min, washed twice in PBS, and then visualized using an SP8 confocal microscope (Leica).

Analysis of embryo ATP level modulation after co-incubation with human EVs

To analyze the impact of EVs in embryo bioenergetics modulation, EF samples (n=5) in phase IV of the menstrual cycle were pooled, and their EV populations were isolated as described above. Embryos from ten mice were obtained and incubated until day E3.5, when only hatching embryos were co-incubated with isolated EF-derived EVs overnight. The following day, embryos were washed in PBS, collected in 1µL PBS, and passed into 96-well opaque plates (Sigma-Aldrich, ref: CLS3917-100EA) in 50 µL H_2O. Replicates of ten good-quality embryos were employed, achieving six replicates (n=60) for ABs and MVs, five for EXOs and all EVs conditions, and three for fresh G2 condition media. 1 µL PBS was

included in duplicate in 50 µL H_2O as a control of the embryo transport vehicle, and an ATP standard curve was generated with fifteen total ATP points from 5 fmol to 50 pmol in duplicate (including a blank) in 50 µL H_2O. ATP measurements were carried out using an ATP bioluminescent somatic cell assay kit (FLASC, Sigma), adapting the protocol from previous studies of human/murine blastomeres and oocytes (van Blerkom et al., 1995; Stojkovic et al., 2001). Stock solutions were prepared following the manufacturer's instructions. The reaction mix was prepared by diluting FLAAM working solution 1:10 in FLAAB and incubating for 5 min at 28°C in the dark. Samples on the plate were added 100 µL 1X ice-cold FLSAR, incubated for 5' at 4°C, and continued processing in a ClarioStar BMG Labtech (BMG Labtech, Germany, Software Version 5.21.R2). The device dispensed 100 µL reaction mix and measured luminescence produced by the luciferase reporter system in consecutive cycles of 1.8 s reaction mix injection, 2 s shaking, and 2 s measurement. The gain was adjusted with the higher ATP standard.

Mitochondrial function assays in embryos

The Seahorse XFe96 Extracellular Flux Analyzer instrument (Agilent) was used to measure the OCR of cultured murine embryos. Hatching/hatched stage embryos were incubated with pre-receptive (P+2; n=4) and receptive stage (P+5; n=5) EF-derived EVs [P+2 derived EXOs (n=4; total embryos: 110); P+2 derived MVs (n=4; total embryos: 130); P+5 derived EXOs (n=4; total embryos: 120); P+5 derived MVs (n=5; total embryos: 150) overnight. Embryos incubated without EVs were used as a control group (n=6; total embryos: 160), while blocked embryos were used as negative control (n=3; total embryos: 120). A total of 720 murine embryos were used for this experiment. Embryos were seeded at ten embryos/well with XF DMEM medium containing 10 mM glucose, 2 mM L-glutamine, and 1 mM pyruvate and stimulated sequentially with 1 µM oligomycin, 1.5 µM carbonyl cyanide-p-trifluoromethoxyphenylhydrazone (FCCP), and 0.5 µM rotenone + antimycin A. Three/four replicates per condition were used in each experiment.

Data analysis

ZetaSizer Nano corresponding to particle concentrations for different EV populations were obtained as an average value from five independent measures of random NTA fields. The standard error for different measures was calculated and represented for each curve as an indicator of the evenness of particles across the sample.

643 To evaluate variation in vesicle concentration throughout the menstrual cycle, concentration
644 data for different samples were uploaded into R software, and the Kruskal-Wallis algorithm
645 was used to detect differences.

646 ANOVA test, Statistical analysis, and Tukey multiple pairwise-comparisons test were used
647 for conditions comparison in ATP content of murine embryos, mitochondrial respiration
648 assays in Seahorse instrument experiments, and mtDNA copy number in EVs. Normal
649 distribution in the study groups was assumed, and P-values <0.05 were considered
650 significant.

651

652 **Acknowledgments**

653 This work was supported by FIS projects from the Spanish Instituto de Salud Carlos III
654 (ISCIII) [PI18/00957 and PI21/00528] to FV and [PI21/00235] to IM. DB was supported by a
655 Formación de Personal Universitario grant [FPU15/02248] by the Spanish Ministerio de
656 Educación, Cultura y Deporte. JGF was supported by Contratos Predoctorales de Formación
657 en Investigación en Salud (PFIS) from ISCIII [FI19/00159]. FV was supported by Miguel
658 Servet Program Type II of ISCIII [CPII18/00020].

659 **Author contributions**

660 DB, CS, and FV designed the study; CS, PF, MAC, and JJE obtained samples; DB, JMA,
661 JGF, CM, and FV performed the research; DB, JMA, AMS, IM, AD, CS, DKG, and FV
662 analyzed data; DB, JMA, CS, and FV wrote the paper; all authors approved the final
663 manuscript, CS and FV contributed to fundraising for the research.

664 **Declaration of interest**

665 The authors declare no conflicts of interest.

666 **References**

667 Andaloussi SE, Mäger I, Breakefield XO, Wood MJA. 2013. Extracellular vesicles: biology
668 and emerging therapeutic opportunities. *Nat Rev Drug Discov* 12:347–357.
669 doi:10.1038/nrd3978

Antonyak MA, Li B, Boroughs LK, Johnson JL, Druso JE, Bryant KL, Holowka DA, Cerione RA. 2011. Cancer cell-derived microvesicles induce transformation by transferring tissue transglutaminase and fibronectin to recipient cells. *Proceedings of the National Academy of Sciences* 108:4852–4857. doi:10.1073/pnas.1017667108

Ashary N, Tiwari A, Modi D. 2018. Embryo Implantation: War in Times of Love. *Endocrinology* 159:1188–1198. doi:10.1210/en.2017-03082

Balkom BWM van, Eisele AS, Pegtel DM, Bervoets S, Verhaar MC. 2015. Quantitative and qualitative analysis of small RNAs in human endothelial cells and exosomes provides insights into localized RNA processing, degradation and sorting. *Journal of Extracellular Vesicles* 4:26760.

Bergsmedh A, Szeles A, Henriksson M, Bratt A, Folkman MJ, Spetz AL, Holmgren L. 2001. Horizontal transfer of oncogenes by uptake of apoptotic bodies. *Proc Natl Acad Sci U S A* 98:6407–6411. doi:10.1073/pnas.101129998

Bidarimath M, Khalaj K, Kridli RT, Kan FWK, Koti M, Tayade C. 2017. Extracellular vesicle mediated intercellular communication at the porcine maternal-fetal interface: A new paradigm for conceptus-endometrial cross-talk. *Sci Rep* 7:40476. doi:10.1038/srep40476

Burns G, Brooks K, Wildung M, Navakanitworakul R, Christenson LK, Spencer TE. 2014. Extracellular vesicles in luminal fluid of the ovine uterus. 9:e90913. doi:10.1371/journal.pone.0090913.s004

Burns GW, Brooks KE, Spencer TE. 2016. Extracellular Vesicles Originate from the Conceptus and Uterus During Early Pregnancy in Sheep. *Biology of reproduction* 94:56. doi:10.1095/biolreprod.115.134973

Chinnery PF, Hudson G. 2013. Mitochondrial genetics. *Brit Med Bull* 106:135–159. doi:10.1093/bmb/ldt017

Clancy JW, Sedgwick A, Rosse C, Muralidharan-Chari V, Raposo G, Method M, Chavrier P, D'Souza-Schorey C. 2015. Regulated delivery of molecular cargo to invasive tumour-derived microvesicles. *Nature Communications* 6:6919. doi:10.1126/science.1102026

Desrochers LM, Bordeleau FC, Reinhart-King CA, Antonyak MA, Cerione RA. 2016. Microvesicles provide a mechanism for intercellular communication by embryonic stem cells during embryo implantation. *Nature Communications* 7:1–11. doi:10.1038/ncomms11958

Díaz-Gimeno P, Horcajadas JA, Martínez-Conejero JA, Esteban FJ, Alamá P, Pellicer A, Simón C. 2011. A genomic diagnostic tool for human endometrial receptivity based on the transcriptomic signature. *Fertility and sterility* 95:50–60, 60 e1–15. doi:10.1016/j.fertnstert.2010.04.063

Diez-Juan A, Rubio C, Marin C, Martínez S, Al-Asmar N, Riboldi M, Díaz-Gimeno P, Valbuena D, D CSMDP. 2015. Mitochondrial DNA content as a viability score in human

euploid embryos: less is better. *Fertility and sterility* 104:534-541.e1. doi:10.1016/j.fertnstert.2015.05.022

Ehnfors J, Kost-Alimova M, Persson NL, Bergsmedh A, Castro J, Levchenko-Tegnebratt T, Yang L, Panaretakis T, Holmgren L. 2009. Horizontal transfer of tumor DNA to endothelial cells in vivo 16:749–757. doi:10.1038/cdd.2009.7

Gardner DK. 2015. Lactate production by the mammalian blastocyst: Manipulating the microenvironment for uterine implantation and invasion? *Bioessays* 37:364–371. doi:10.1002/bies.201400155

Gardner DK, Harvey AJ. 2015. Blastocyst metabolism. *Reproduction Fertility Dev* 27:638. doi:10.1071/rd14421

Greening DW, Nguyen HPT, Elgass K, Simpson RJ, Salamonsen LA. 2016. Human Endometrial Exosomes Contain Hormone-Specific Cargo Modulating Trophoblast Adhesive Capacity: Insights into Endometrial-Embryo Interactions. *Biol Reprod* 94:Article 38, 1-15. doi:10.1095/biolreprod.115.134890

Gross N, Kropp J, Khatib H. 2017. MicroRNA Signaling in Embryo Development. *Biology* 6:34. doi:10.3390/biology6030034

Guescini M, Guidolin D, Vallorani L, Casadei L, Gioacchini AM, Tibollo P, Battistelli M, Falcieri E, Battistin L, Agnati LF, Stocchi V. 2010. C2C12 myoblasts release micro-vesicles containing mtDNA and proteins involved in signal transduction. *Exp Cell Res* 316:1977–1984. doi:10.1016/j.yexcr.2010.04.006

Gurner KH, Evans J, Hutchison JC, Harvey AJ, Gardner DK. 2022. A microenvironment of high lactate and low pH created by the blastocyst promotes endometrial receptivity and implantation. *Reprod Biomed Online* 44:14–26. doi:10.1016/j.rbmo.2021.09.012

Holmgren L, Szeles A, Rajnavölgyi E, Folkman J, Klein G, Ernberg I, Falk KI. 1999. Horizontal transfer of DNA by the uptake of apoptotic bodies. *Blood* 93:3956–3963.

Huang X, Yuan T, Tschannen M, Sun Z, Jacob H, Du M, Liang Meihua, Dittmar RL, Liu Y, Liang Mingyu, Kohli M, Thibodeau SN, Boardman L, Wang L. 2013. Characterization of human plasma-derived exosomal RNAs by deep sequencing. *BMC genomics* 14:319. doi:10.1186/1471-2164-14-319

Kawamura Y, Yamamoto Y, Sato T, Ochiya T. 2017. Extracellular vesicles as trans□genomic agents: Emerging roles in disease and evolution. *Cancer Sci* 108:824–830. doi:10.1111/cas.13222

Kumar D, Gupta D, Shankar S, Srivastava RK. 2014. Biomolecular characterization of exosomes released from cancer stem cells: Possible implications for biomarker and treatment of cancer. *Oncotarget* 6:3280–3291. doi:10.18632/oncotarget.2462

Lázaro-Ibáñez E, Sanz-Garcia A, Visakorpi T, Escobedo-Lucea C, Siljander P, Ayuso-Sacido Á, Yliperttula M. 2014. Different gDNA content in the subpopulations of prostate cancer

745 extracellular vesicles: Apoptotic bodies, microvesicles, and exosomes. *The Prostate*
746 74:1379–1390. doi:10.1002/pros.22853

747 Lee B, Saadeldin I, Oh HJ. 2015. Embryonic–maternal cross-talk via exosomes:
748 potential implications. *Stem Cells and Cloning: Advances and Applications* 103.
749 doi:10.2147/sccaa.s84991

750 Liang J, Wang S, Wang Z. 2017. Role of microRNAs in embryo implantation. *Reprod Biol*
751 *Endocrin* 15:90. doi:10.1186/s12958-017-0309-7

752 Ng YH, Rome S, Jalabert A, Forterre A, Singh H, Hincks CL, Salamonsen LA. 2013.
753 Endometrial Exosomes/Microvesicles in the Uterine Microenvironment: A New Paradigm
754 for Embryo-Endometrial Cross Talk at Implantation. *Plos One* 8:e58502.
755 doi:10.1371/journal.pone.0058502

756 Niel G van, D'Angelo G, Raposo G. 2018. Shedding light on the cell biology of extracellular
757 vesicles. *Nat Rev Mol Cell Bio* 19:213–228. doi:10.1038/nrm.2017.125

758 Ruiz-González I, Xu J, Wang X, Burghardt RC, Dunlap KA, Bazer FW. 2015. Exosomes,
759 endogenous retroviruses and toll-like receptors: pregnancy recognition in ewes.
760 *Reproduction* 149:281–291. doi:10.1530/rep-14-0538

761 Salomon C, Yee S, Scholz-Romero K, Kobayashi M, Vaswani K, Kvaskoff D, Illanes SE,
762 Mitchell MD, Rice GE. 2014. Extravillous trophoblast cells-derived exosomes promote
763 vascular smooth muscle cell migration. *Frontiers in pharmacology* 5:175.
764 doi:10.3389/fphar.2014.00175

765 Sansone P, Savini C, Kurelac I, Chang Q, Amato LB, Strillacci A, Stepanova A, Iommarini
766 L, Mastroleo C, Daly L, Galkin A, Thakur BK, Soplop N, Uryu K, Hoshino A, Norton L,
767 Bonafé M, Cricca M, Gasparre G, Lyden D, Bromberg J. 2017. Packaging and transfer of
768 mitochondrial DNA via exosomes regulate escape from dormancy in hormonal therapy-
769 resistant breast cancer. *Proc National Acad Sci* 114:E9066–E9075.
770 doi:10.1073/pnas.1704862114

771 Simón C, Greening DW, Bolumar D, Balaguer N, Salamonsen LA, Vilella F. 2018.
772 Extracellular Vesicles in Human Reproduction in Health and Disease. *Endocrine reviews*
773 39:292–332. doi:10.1210/er.2017-00229

774 Taanman J-W. 1999. The mitochondrial genome: structure, transcription, translation and
775 replication. *Biochimica Et Biophysica Acta Bba - Bioenergetics* 1410:103–123.
776 doi:10.1016/s0005-2728(98)00161-3

777 Thakur BK, Zhang H, Becker A, Matei I, Huang Y, Costa-Silva B, Zheng Y, Hoshino A,
778 Brazier H, Xiang J, Williams C, Rodriguez-Barrueco R, Silva JM, Zhang W, Hearn S,
779 Elemento O, Paknejad N, Manova-Todorova K, Welte K, Bromberg J, Peinado H, Lyden
780 D. 2014a. Double-stranded DNA in exosomes: a novel biomarker in cancer detection. *Cell*
781 *Res* 24:766–769. doi:10.1038/cr.2014.44

782 Thakur BK, Zhang H, Becker A, Matei I, Huang Y, Costa-Silva B, Zheng Y, Hoshino A,
783 Brazier H, Xiang J, Williams C, Rodriguez-Barrueco R, Silva JM, Zhang W, Hearn S,

Elemento O, Paknejad N, Manova-Todorova K, Welte K, Bromberg J, Peinado H, Lyden D. 2014b. Double-stranded DNA in exosomes: a novel biomarker in cancer detection. *Cell research* 24:766–769. doi:10.1038/cr.2014.44

Tong M, Chamley LW. 2015. Placental extracellular vesicles and feto-maternal communication. *Cold Spring Harbor perspectives in medicine* 5:a023028. doi:10.1101/cshperspect.a023028

Torralba D, Baixauli F, Villarroya-Beltri C, Fernández-Delgado I, Latorre-Pellicer A, Acín-Pérez R, Martín-Cófreces NB, Jaso-Tamame ÁL, Iborra S, Jorge I, González-Aseguinolaza G, Garaude J, Vicente-Manzanares M, Enríquez JA, Mittelbrunn M, Sánchez-Madrid F. 2018. Priming of dendritic cells by DNA-containing extracellular vesicles from activated T cells through antigen-driven contacts. *Nat Commun* 9:2658. doi:10.1038/s41467-018-05077-9

Valadi H, Ekström K, Bossios A, Sjöstrand M, Lee JJ, Lötvall JO. 2007. Exosome-mediated transfer of mRNAs and microRNAs is a novel mechanism of genetic exchange between cells. *Nature cell biology* 9:654–659. doi:10.1038/ncb1596

Vilella F, Moreno-Moya JM, Balaguer N, Grasso A, Herrero M, Martinez S, Marcilla A, Simón C. 2015. Hsa-miR-30d, secreted by the human endometrium, is taken up by the pre-implantation embryo and might modify its transcriptome. *Development (Cambridge, England)* 142:3210–3221. doi:10.1242/dev.124289

Villarroya-Beltri C, Guti C, Sanchez-Cabo F, Perez-Hernandez D, Vazquez J, Martin-Cofreces N, Martinez-Herrera DJ, Pascual-Montano A, Mittelbrunn M, Sanchez-Madrid F. 2013. Sumoylated hnRNPA2B1 controls the sorting of miRNAs into exosomes through binding to specific motifs. *Nature Communications* 4:1–10. doi:10.1038/ncomms3980

Vojtech L, Woo S, Hughes S, Levy C, Ballweber L, Sauteraud RP, Strobl J, Westerberg K, Gottardo R, Tewari M, Hladik F. 2014. Exosomes in human semen carry a distinctive repertoire of small non-coding RNAs with potential regulatory functions. *Nucleic Acids Research* 42:7290–7304. doi:10.1093/nar/gku347

Waldenström A, Gennebäck N, Hellman U, Ronquist G. 2012. Cardiomyocyte microvesicles contain DNA/RNA and convey biological messages to target cells. 7:e34653. doi:10.1371/journal.pone.0034653

Waterhouse M, Themeli M, Bertz H, Zoumbos N, Finke J, Spyridonidis A. 2011. Horizontal DNA Transfer from Donor to Host Cells as an Alternative Mechanism of Epithelial Chimerism after Allogeneic Hematopoietic Cell Transplantation. *Biology of Blood and Marrow Transplantation* 17:319–329. doi:10.1016/j.bbmt.2010.09.001

Youle RJ, Narendra DP. 2011. Mechanisms of mitophagy. *Nat Rev Mol Cell Bio* 12:9–14. doi:10.1038/nrm3028

Figure Titles and Legends

Figure 1. Characterization of endometrial fluid-derived extracellular vesicles. (**A-I**) Analysis of ABs, MVs, and EXOs isolated from human EF samples: morphology by TEM (**A**, **D**, and **G**), size distribution by DLS (**B**, **E**, and **H**), and protein marker expression by Western blotting (**C**, **F**, and **I**). TEM images obtained using two different protocols for an external (deposition processing, upper images) or internal (ultrathin slide processing, lower images) view of EVs. Size distribution analyzed in a single EF sample by DLS during the receptive phase for (**B**) ABs, (**E**) MVs, and (**H**) EXOs. Graphs show the average size distribution and percentage of total particles contained within the populations. Specific protein markers analyzed by Western blotting for (**C**) ABs, (**F**) MVs, and (**I**) EXOs. Analyzed markers (and associated molecular mass) were calnexin (90–100 kDa), calreticulin (60 kDa), VDAC1 (31 kDa), ARF6 (18 kDa), CD9 (24 kDa), CD63 (30–60 kDa), and TSG101 (45–50 kDa). (**J** and **K**) Particle concentration and size distribution measured by NTA for (**J**) MVs and (**K**) EXOs secreted throughout the menstrual cycle. One-way ANOVA and Kruskal-Wallis rank sum tests performed to compare the distinct menstrual cycle phases - no significant differences were observed.

Figure 2. DNA sequencing analysis and coding sequence comparisons of human endometrial fluid-derived extracellular vesicle populations. (**A** and **B**) Volcano plots comparing DNA sequence enrichment between ABs, MVs, and EXOs. Only MVs show significant sequence enrichment compared to ABs and EXOs. (**C**) Specific gene ID DNA sequences encapsulated within MVs compared to ABs and EXOs, which are mainly mitochondrial DNA.

Figure 3. Quantification of mitochondrial DNA in human endometrial tissues and human endometrial fluid-derived microvesicles. (**A**) Relative mtDNA/nDNA ratio calculated from endometrial biopsies from donors undergoing HRT in pre-receptive (P+2), receptive (P+5), and post-receptive (P+8) periods. (**B**) Gene expression analysis of endometrial biopsies for nuclear genes coding for mitophagy- and mtDNA packing-related proteins (upper panel) and for genes coding for proteins related to mitochondrial function (lower panel). (**C**) Quantification of relative mtDNA copy number packed into MVs isolated from the EF in pre-receptive, receptive, and post-receptive periods. One-way ANOVA and Kruskal-Wallis rank sum tests performed to compare the distinct periods - no significant differences were observed.

Figure 4. Internalization of endometrial extracellular vesicle-derived DNA by cells of the murine embryo. Confocal images show hatched embryos after co-culture with EdU-tagged ABs, MVs, and EXOs isolated from Ishikawa cell supernatants. Embryo membranes were visualized with Wheat germ agglutinin (WGA) in red, embryo nuclei with DAPI, and EdU-tagged transferred DNA in green. Zoomed images taken from the areas demarcated by white boxes in merge images. Cell-free DNA and residual small-sized EVs were used as control conditions (Neg). Scale bar in zoom = 20 µm

Figure 5. Mitochondrial function in embryos incubated with human endometrial fluid-derived extracellular vesicles. (**A**) Murine embryo ATP content after overnight co-incubation with the EF-derived EV populations (phase IV or receptive phase of the natural menstrual cycle). "All EVs" indicates a combination of ABs, MVs, and EXOs. Embryos not incubated with EVs used as a control condition (Cnt). (**B**) OCR was recorded on a Seahorse instrument before and after drug injection (timing indicated on the graph). Blocked embryos used as an additional negative control (Neg Cnt). (**C**) Basal respiration [(Last rate measurement before the first injection)-(minimum rate measurement after Rotenone/antimycin A injection)] and (**D**) Maximal respiration [(Maximal rate measurement after FCCP injection)-(minimum rate measurement after Rotenone/antimycin A injection)] shown for each condition. One-way ANOVA and Tukey comparison post-hoc performed - no significant differences between conditions were observed (excluding the Neg Cnt condition).

Supplemental Information Titles and Legends

Supplementary Figure 1. Transmission electron micrograph analysis of human endometrial fluid-derived extracellular vesicle morphology. TEM micrographs show morphological details of human EF (**A** and **B**) ABs, (**C**) MVs, and (**D**) EXOs. Images obtained via two different protocols to obtain an external (deposition processing) and internal (ultrathin slide processing) view. Isolated ABs displayed a wide range of vesicle sizes (>1 µm to <50 nm) with heterogeneous content composition, including membranous structures within ABs (**B3**). Image **B2** corresponds to a higher magnification of image **B1**. MVs were considerably more abundant, with sizes from 200–700 nm (**C1** and **C2**) with highly electron-dense heterogeneous contents (**C3** and **C4**). EXOs displayed a similar aspect and abundance to MVs (**D**) with sizes of 40–160 nm but more homogeneous structures.

884 **Supplementary Figure 2. Size distribution of human endometrial fluid-derived**
885 **microvesicles and exosomes measured by nanoparticle tracking analysis.** Size patterning
886 and total particle concentration of isolated (**A**) MVs and (**B**) EXOs obtained from a single
887 human EF sample isolated during the receptive phase of the menstrual cycle. The standard
888 error of five measurements shown as the grey area in each graph.

889 **Supplementary Figure 3. Microvesicle and exosome dynamics in endometrial fluid**
890 **samples isolated during the menstrual cycle.** Particle concentration and size distribution by
891 NTA for (**A**) MVs and (**B**) EXOs analyzed throughout the menstrual cycle.

892 **Supplementary Figure 4. Effect of DNase treatment in sequencing analysis and coding**
893 **sequences comparison between human endometrial fluid-derived extracellular vesicle**
894 **populations.** Sequencing analysis results for (**A**) ABs and (**B**) EXOs treated with (+ DNase)
895 and without (- DNase) DNase type I. (**A** and **B**; Left Panels) PCA analyses show grouping
896 due to DNase treatment for both ABs and EXOs. (**A** and **B**; Right Panels) Volcano plots
897 show the significant enrichment of DNA sequences in treated EVs (purple dots in volcano
898 plots) versus untreated EVs (yellow dots in volcano plots). (**C**) Principal component analysis
899 shows EV sample grouping due to specificity in coding-gene sequences.

900 **Supplementary Figure 5. Characterization of EdU-tagged DNA incorporation into**
901 **extracellular vesicles isolated from Ishikawa cells.** EXOs, MVs, and ABs isolated from
902 non-EdU-tagged (Control) and EdU-tagged DNA (EdU-DNA) were analyzed by flow
903 cytometry for complexity (SSC-A) and EdU-488 staining (FITC-A). Gates show positive
904 EdU-488 EVs percentage in the distinct populations.

905 **Supplementary Figure 6. Z-stack/orthogonal sections of murine embryos co-cultured**
906 **with extracellular vesicles containing EdU-tagged DNA**. Images show hatching/hatched
907 embryos after co-culture with EdU-tagged EVs (ABs, MVs, and EXOs). White arrows show
908 the co-localization of tagged DNA and nuclei, indicating the nuclear location of extracellular
909 vesicle-derived DNA. Embryo membranes are visualized with WGA in red, embryo nuclei
910 with DAPI, and EdU-tagged transferred DNA in green. Cell-free DNA and residual small-
911 sized EVs were used as control conditions (Neg). Bar = 20 µm. Red lines indicate the
912 intersection for orthogonal image acquisition.

913 **Supplementary Figure 7. Detection of exogenous mitochondrial DNA in mouse**
914 **embryos.** Embryos co-incubated with 10 µM of an ATP8 DNA sequence (mtDNA fragment)

915 conjugated with Biotin overnight ATP8-Biotin DNA were detected with streptavidin-Cy3
916 (Green) and nuclei counterstained with DAPI (Blue). Negative control embryos incubated
917 without the ATP8-Biotin show the background signal after streptavidin-Cy3 staining.

918

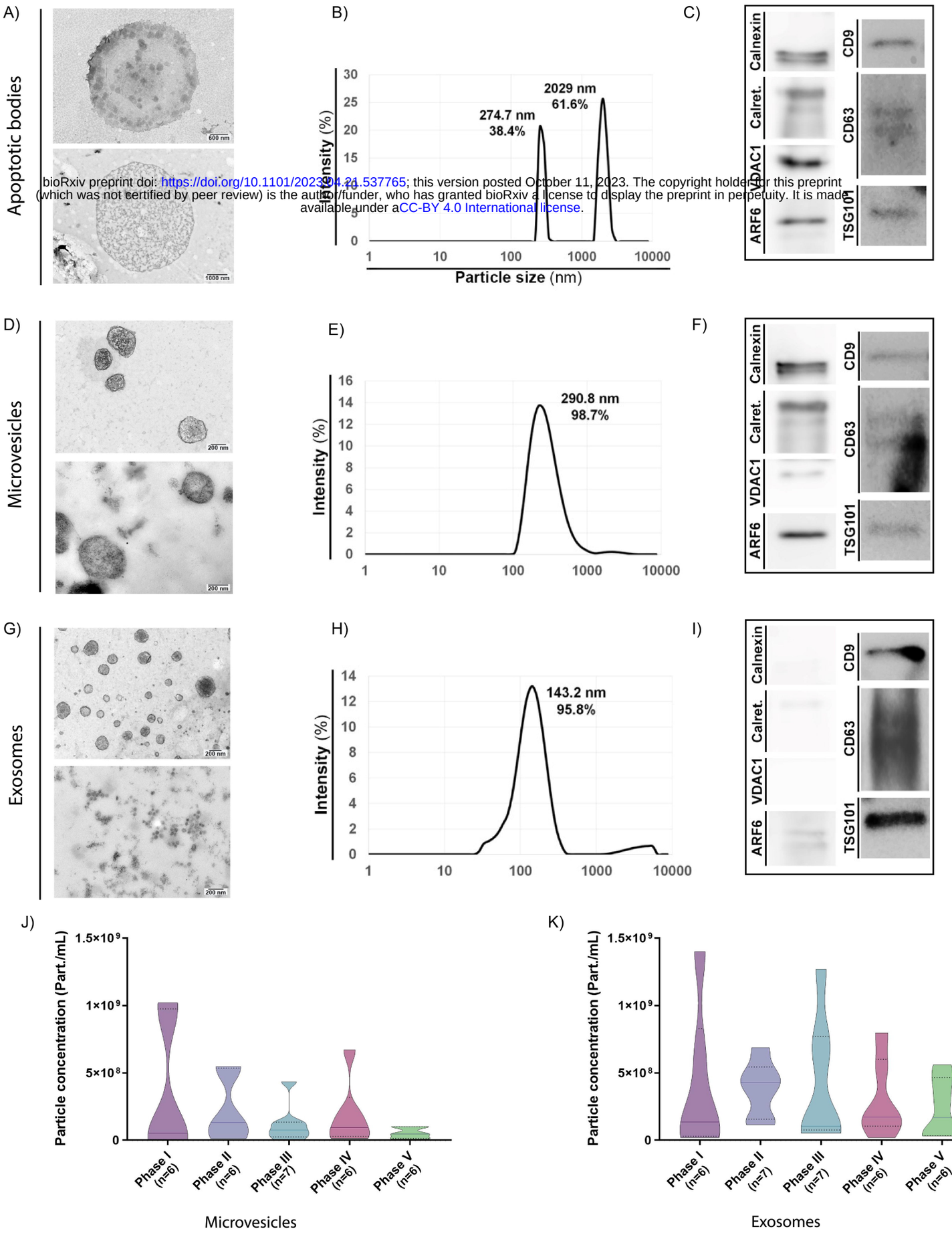

Figure 1. Characterization of endometrial fluid-derived extracellular vesicles. (**A-I**) Analysis of ABs, MVs, and EXOs isolated from human EF samples: morphology by TEM (**A**, **D**, and **G**), size distribution by DLS (**B**, **E**, and **H**), and protein marker expression by Western blotting (**C**, **F**, and **I**). TEM images obtained using two different protocols for an external (deposition processing, upper images) or internal (ultrathin slide processing, lower images) view of EVs. Size distribution analyzed in a single EF sample by DLS during the receptive phase for (**B**) ABs, (**E**) MVs, and (**H**) EXOs. Graphs show the average size distribution and percentage of total particles contained within the populations. Specific protein markers analyzed by Western blotting for (**C**) ABs, (**F**) MVs, and (**I**) EXOs. Analyzed markers (and associated molecular mass) were calnexin (90–100 kDa), calreticulin (60 kDa), VDAC1 (31 kDa), ARF6 (18 kDa), CD9 (24 kDa), CD63 (30–60 kDa), and TSG101 (45–50 kDa). (**J** and **K**) Particle concentration and size distribution measured by NTA for (**J**) MVs and (**K**) EXOs secreted throughout the menstrual cycle. One-way ANOVA and Kruskal-Wallis rank sum tests performed to compare the distinct menstrual cycle phases - no significant differences were observed.

A)

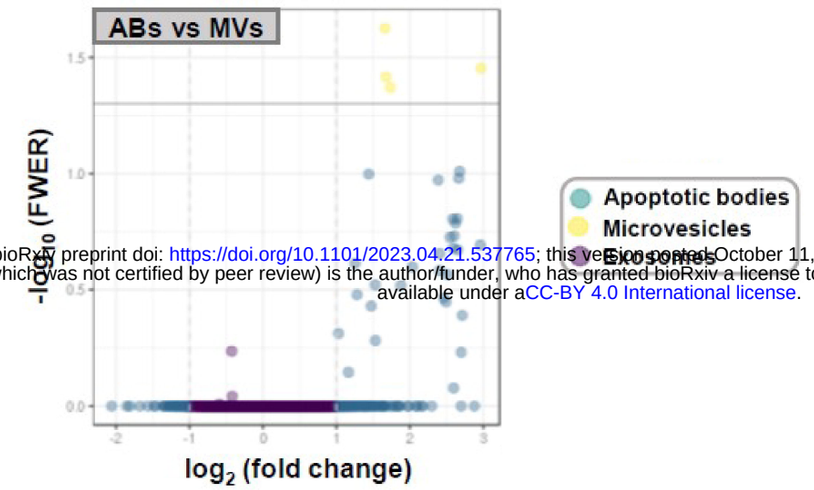

B)

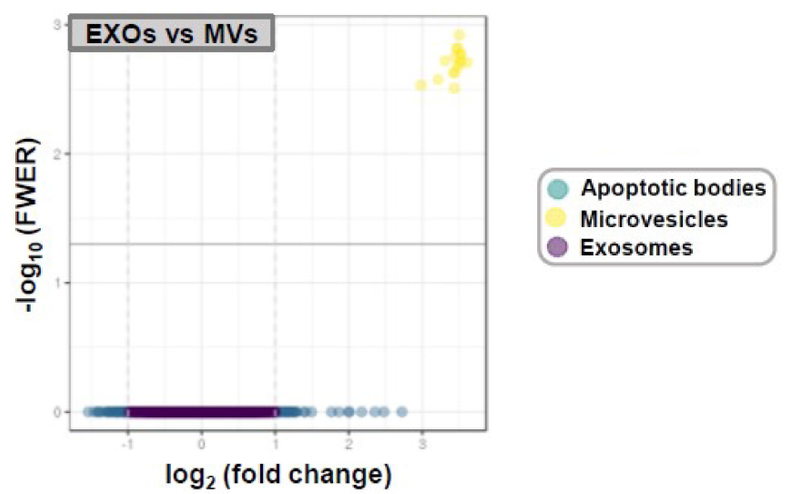

C)

Comparison	Gene ID	Fold-Change	Chr	Gene Type	Encoded product
DNA cargo of MVs Vs EXOs	MT-ATP8	12.22	MT	Protein coding	ATP Synthase 8
	MT-ND2	11.51	MT	Protein coding	NADH dehydrogenase 8
	MTND2P28	11.49	1	Pseudogene	MT-DN2 pseudogene 28
	MT-CO2	11.47	MT	Protein coding	Cytochrome C oxidase II
	MT-CYB	11.42	MT	Protein coding	Cytochrome B
	MT-ND3	11.34	MT	Protein coding	NADH dehydrogenase 3
	MT-ND6	11.16	MT	Protein coding	NADH dehydrogenase 6
	MT-CO3	11.16	MT	Protein coding	Cytochrome c oxidase III
	MT-ND5	11.08	MT	Protein coding	NADH dehydrogenase 5
	MT-ND4	10.89	MT	Protein coding	NADH dehydrogenase 4
	MT-ND1	10.88	MT	Protein coding	NADH dehydrogenase 1
	MT-ATP6	10.83	MT	Protein coding	ATP synthase 6
	MT-CO1	10.76	MT	Protein coding	Cytochrome c oxidase I
	MT-ND4L	9.91	MT	Protein coding	NADH dehydrogenase 4L
	MTATP6P1	9.29	1	Pseudogene	ATP synthase 6 pseudogene 1
	RP5-857K21.4	7.91	1	lincRNA	---
DNA cargo of MVs Vs ABs	MTND2P28	7.83	1	Pseudogene	MT-DN2 pseudogene 28
	CCDC177	3.33	14	Protein coding	Coiled-Coil Domain Containing 177
	GAS1	3.19	9	Protein coding	Growth arrest-specific 1
	MESDC1	3.17	15	Protein coding	Mesoderm development candidate 1

Figure 2. DNA sequencing analysis and coding sequence comparisons of human endometrial fluid-derived extracellular vesicle populations. (**A** and **B**) Volcano plots comparing DNA sequence enrichment between ABs, MVs, and EXOs. Only MVs show significant sequence enrichment compared to ABs and EXOs. (**C**) Specific gene ID DNA sequences encapsulated within MVs compared to ABs and EXOs, which are mainly mitochondrial DNA.

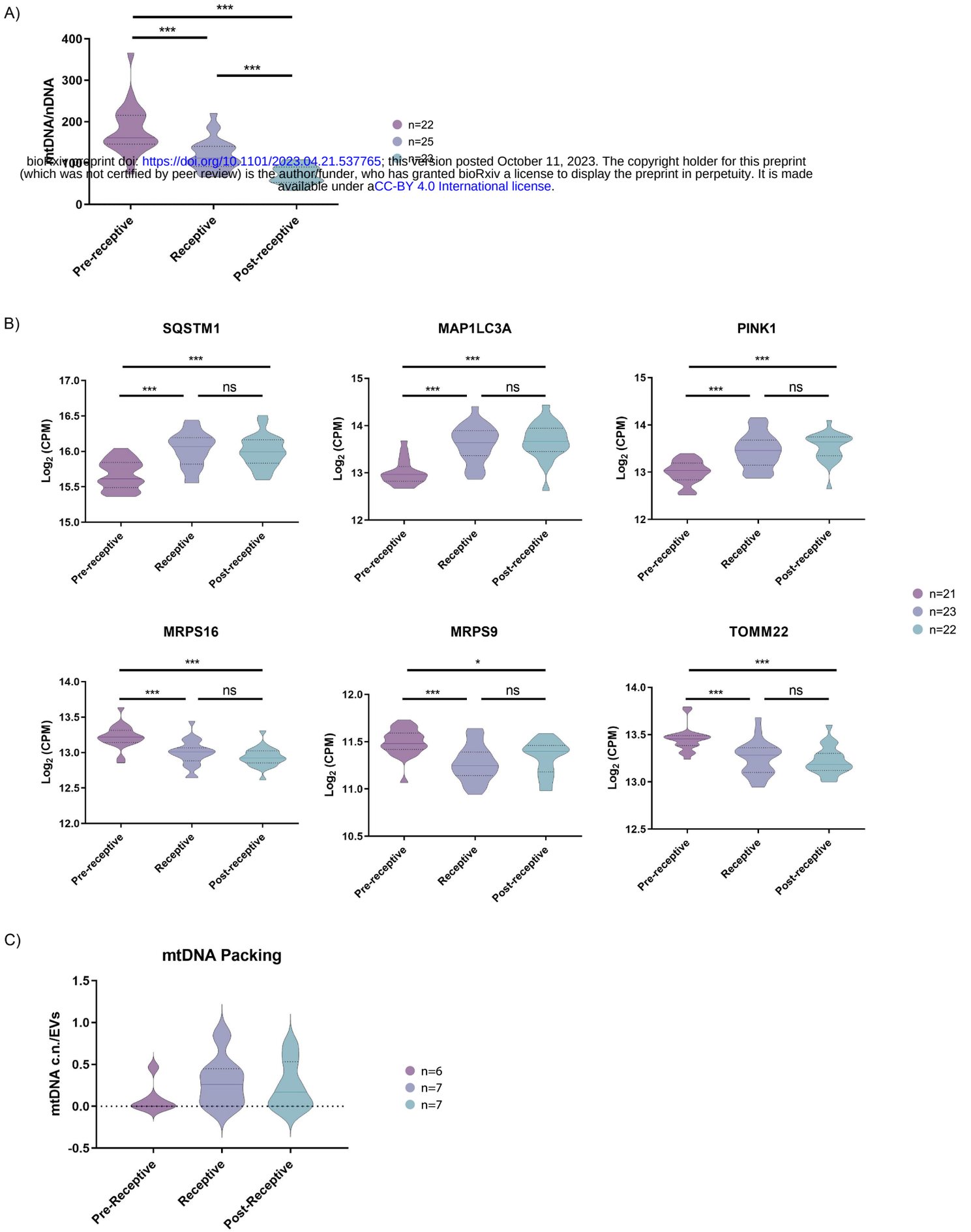

Figure 3. Quantification of mitochondrial DNA in human endometrial tissues and human endometrial fluid-derived microvesicles. (**A**) Relative mtDNA/nDNA ratio calculated from endometrial biopsies from donors undergoing HRT in pre-receptive (P+2), receptive (P+5), and post-receptive (P+8) periods. (**B**) Gene expression analysis of endometrial biopsies for nuclear genes coding for mitophagy- and mtDNA packing-related proteins (upper panel) and for genes coding for proteins related to mitochondrial function (lower panel). (**C**) Quantification of relative mtDNA copy number packed into MVs isolated from the EF in pre-receptive, receptive, and post-receptive periods. One-way ANOVA and Kruskal-Wallis rank sum tests performed to compare the distinct periods - no significant differences were observed.

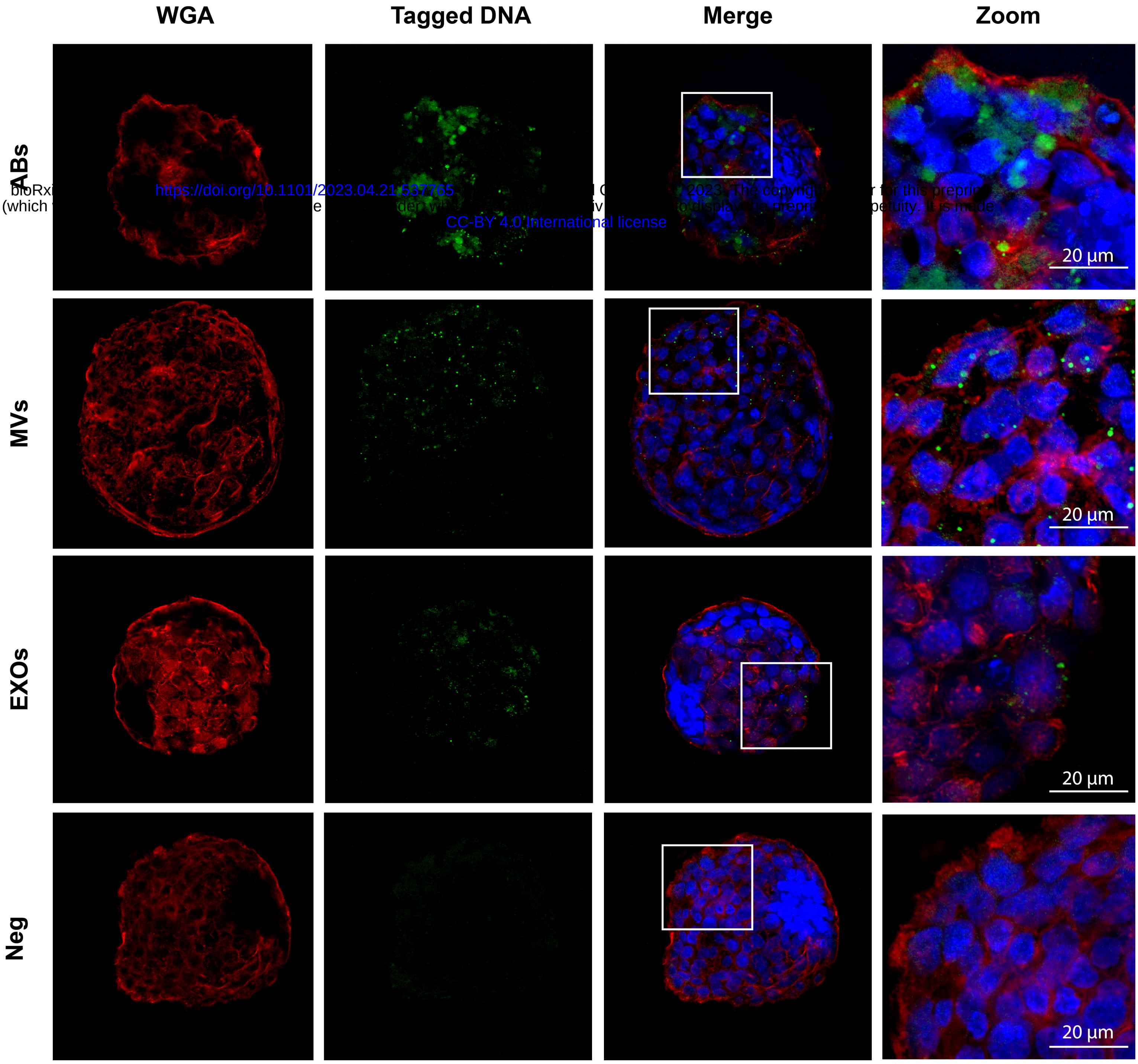

Figure 4. Internalization of endometrial extracellular vesicle-derived DNA by cells of the murine embryo. Confocal images show hatched embryos after co-culture with EdU-tagged ABs, MVs, and EXOs isolated from Ishikawa cell supernatants. Embryo membranes were visualized with Wheat germ agglutinin (WGA) in red, embryo nuclei with DAPI, and EdU-tagged transferred DNA in green. Zoomed images taken from the areas demarcated by white boxes in merge images. Cell-free DNA and residual small-sized EVs were used as control conditions (Neg). Scale bar in zoom = 20 µm

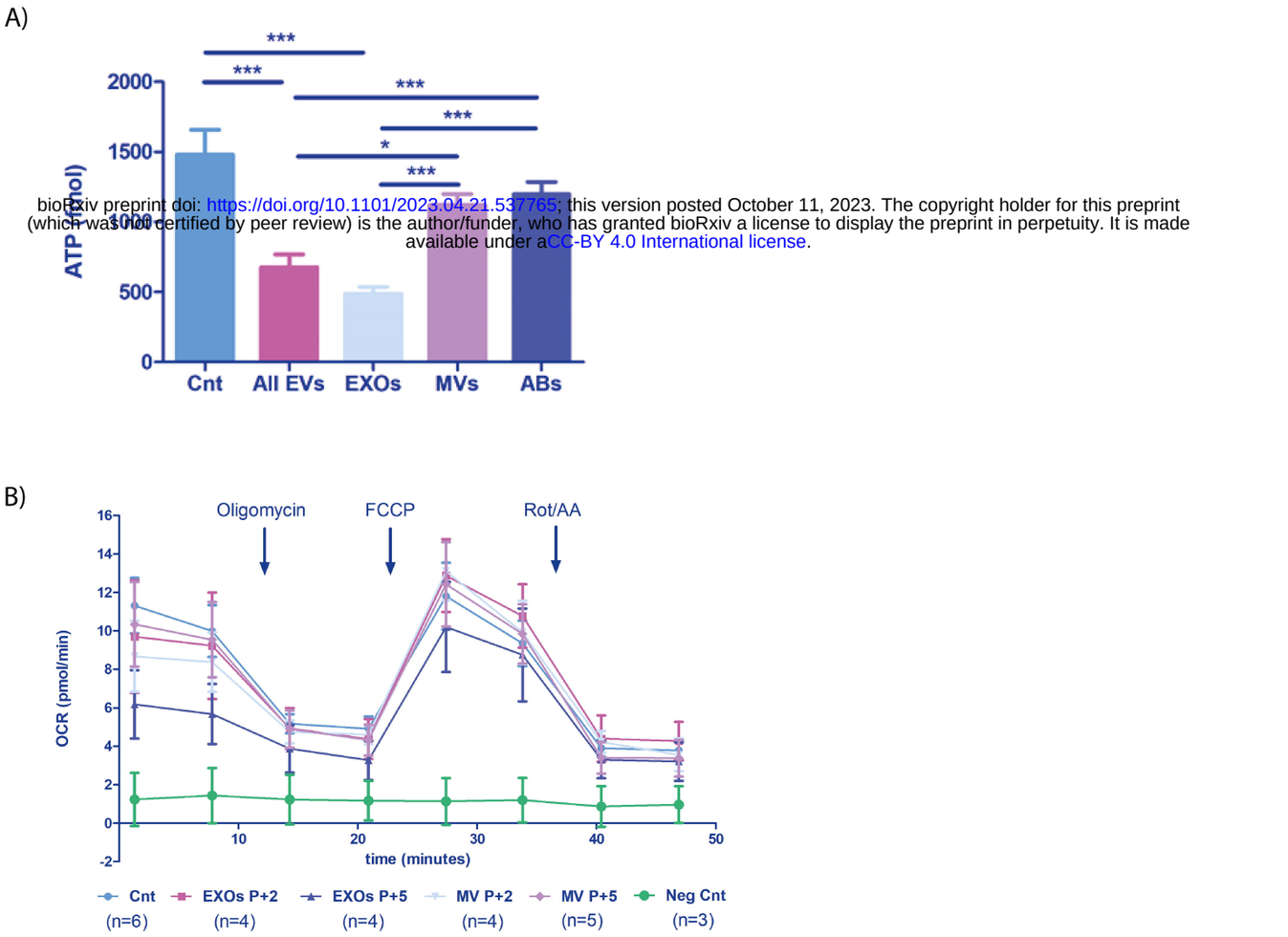

Figure 5. Mitochondrial function in embryos incubated with human endometrial fluid-derived extracellular vesicles. (**A**) Murine embryo ATP content after overnight co-incubation with the EF-derived EV populations (phase IV or receptive phase of the natural menstrual cycle). "All EVs" indicates a combination of ABs, MVs, and EXOs. Embryos not incubated with EVs used as a control condition (Cnt). (**B**) OCR was recorded on a Seahorse instrument before and after drug injection (timing indicated on the graph). Blocked embryos used as an additional negative control (Neg Cnt). (**C**) Basal respiration [(Last rate measurement before the first injection)-(minimum rate measurement after Rotenone/antimycin A injection)] and (**D**) Maximal respiration [(Maximal rate measurement after FCCP injection)-(minimum rate measurement after Rotenone/antimycin A injection)] shown for each condition. One-way ANOVA and Tukey comparison post-hoc performed - no significant differences between conditions were observed (excluding the Neg Cnt condition).